processes

MDPI

Article

A Method for Image-Based Interpretation of the Pulverized Coal Cloud in the Blast Furnace Tuyeres

Guanwei Zhou [1,2], Henrik Saxén [1,*], Olli Mattila [3] and Yaowei Yu [2]

[1] Process and Systems Engineering Laboratory, Faculty of Science and Engineering, Åbo Akademi University, FI-20500 Turku, Finland; guanwei.zhou@abo.fi
[2] State Key Laboratory of Advanced Special Steel, Shanghai Key Laboratory of Advanced Ferrometallurgy, School of Materials Science and Engineering, Shanghai University, Shanghai 200444, China; yaowei.yu@hotmail.com
[3] SSAB Europe Oy, Rautaruukintie 155, FI-92101 Raahe, Finland; olli.mattila@ssab.com
* Correspondence: hsaxen@abo.fi

Abstract: The conditions in the combustion zones, i.e., the raceways, are crucial for the operation of the blast furnace. In recent years, advancements in tuyere cameras and image processing and interpretation techniques have provided a better means by which to obtain information from this region of the furnace. In this study, a comprehensive approach is proposed to visually monitor the status of the pulverized coal cloud at the tuyeres based on a carefully designed processing strategy. Firstly, tuyere images are preprocessed to remove noise and enhance image quality, applying the adaptive Otsu algorithm to detect the edges of the coal cloud, enabling precise delineation of the pulverized coal region. Next, a Swin–Unet model, which combines the strengths of Swin Transformer and U-Net architecture, is employed for accurate segmentation of the coal cloud area. The extracted pulverized coal cloud features are analyzed using RGB super-pixel weighting, which takes into account the variations in color within the cloud region. It is demonstrated that the pulverized coal injection rate shows a correlation with the state of the cloud detected based on the images. The effectiveness of this visual monitoring method is validated using real-world data obtained from a blast furnace of SSAB Europe. The experimental results align with earlier research findings and practical operational experience.

Keywords: blast furnace; pulverized coal injection; image segmentation; Swin–Unet

check for updates

Citation: Zhou, G.; Saxén, H.; Mattila, O.; Yu, Y. A Method for Image-Based Interpretation of the Pulverized Coal Cloud in the Blast Furnace Tuyeres. *Processes* **2024**, *12*, 529. https://doi.org/10.3390/pr12030529

Academic Editor: Raymond Cecil Everson

Received: 8 February 2024
Revised: 26 February 2024
Accepted: 5 March 2024
Published: 6 March 2024

Copyright: © 2024 by the authors. Licensee MDPI, Basel, Switzerland. This article is an open access article distributed under the terms and conditions of the Creative Commons Attribution (CC BY) license (https://creativecommons.org/licenses/by/4.0/).

1. Introduction

The blast furnace (BF) is an important unit within the processes in the steel industry for iron production. The combustion reactions in the lower part of the furnace generate large amounts of heat and reducing gases, providing the necessary conditions for the smelting and reduction processes in the upper parts. As injecting pulverized coal (PC) is the main approach to reduce coke consumption, most blast furnaces employ Pulverized Coal Injection (PCI) technology, where pulverized coal conveyed by a carrier gas (typically nitrogen) and hot air ("blast") is injected into the tuyere region and undergo intense combustion [1]. Unburned pulverized coal can lead to a deterioration in the permeability of the furnace and affect the properties of the slag. It also raises the fuel rate. Therefore, determining the combustion state of the pulverized coal at the tuyere is helpful for adjusting the operation of the blast furnace under uncertain conditions, ensuring the complete combustion of pulverized coal, and improving the stability of BF operations.

Shen et al. [2–4] conducted extensive research on the simulation of the blast furnace raceway. They constructed three-dimensional models and delved deeply into how blast parameters, PCI rate, and oxygen enrichment rate in the tuyere area positively influence combustion within the raceway. Dianyu et al. [5] employed a multi-scale approach, combining CFD and EDM, based on granular-level reaction flows in the blast furnace, to study

the internal evolution of the blast furnace raceway. Straka et al. [6] predicted the shape of the raceway under the different blast parameters. Du et al. [7] used a drop-tube furnace to simulate the reactions of PC under BF conditions.

While simulation results provide valuable insights, they often face limitations in terms of computational speed and constraints in experimental simulations. The complex conditions in the raceways, where coke and injected pulverized coal are simultaneously combusted under extreme conditions with a high velocity jet that induces a swirling motion in the coke particles, make it practically impossible to reconstruct the conditions numerically. This makes it challenging to provide model-based real-time guidance for the actual operation of blast furnaces. However, with the development of computer image processing techniques and the application of industrial array CCD devices, visualization technology can provide a more intuitive and real-time reflection of the tuyere conditions. As one of the few means of observing the internal parts of the blast furnace, tuyere cameras provide a unique way of extracting detailed information about the blast and reductant supply, combustion state, and flame characteristics. Such information can be useful for maintaining a stable state in the furnace, detecting imbalances in the blast and coal supply along the periphery, and for controlling the thermal state, which are prerequisites of an efficient and low-emission operation. The main challenge in a manual interpretation is that no operator has the time to monitor the results of tens of cameras simultaneously, and that the interpretation is subjective and rather qualitative. Automatic systems for lance blockage detection based on the CCD have been proposed based on logic concerning the darkness of the image. Zhou et al. [8,9], Cheng et al. [10], and Li et al. [11] investigated the temperature distribution within the tuyere region based on video images. They established both two-dimensional and three-dimensional temperature fields to study the impact of blast conditions and PCI parameters on combustion within the tuyere. Zhang et al. [12] utilized a fixed background template to extract pulverized coal clouds from the images and studied the operational conditions of PCI, as well as the coke particle size distribution within the tuyere region. Huang et al. [13] and Wang et al. [14] addressed the issue of distinguishing between the lance and the pulverized coal cloud caused by similar grayscale values by studying a dynamic background board model. The research mentioned above, based on semantic segmentation of tuyere images, primarily focused on detecting (emerging) lance blockage, and more generic tools are needed to extract information from the tuyere camera images.

The goal of the present work is to build a powerful model for the image-based interpretation of the conditions in the blast furnace tuyere region, enabling the extraction of useful information from the pulverized coal cloud and the assessment of combustion information about raceway. Researchers in this field have mainly applied CNN models for semantic segmentation [15–17]. While traditional CNN models perform well in image segmentation, they are limited in their ability to learn global and long-range semantic interactions due to the constraints of convolutional operations [18]. This limitation becomes more prominent in complex scenarios involving various interferences, such as the variability in camera angles or positions resulting from production adjustments, as well as changes in lance position due to modifications in the coal injection process. It was found that the U-Net and transformer combination was more appropriate for segmentation; an appropriate transformer-based segmentation approach can be applied or the transformer structure can be adjusted in accordance with the segmentation requirements [19]. The Swin–Unet model [20], based on Swin Transformer blocks, is particularly well-suited for handling images with limited spatial information in the context of image segmentation. This paper proposes a pulverized coal cloud detection model based on Swin–Unet, which accurately segments the pulverized coal cloud region and demonstrates superior robustness compared to other methods. The proposed model utilizes the super-pixel RGB-weighted method, which assigns weights to each pixel based on the color differences in the corresponding pulverized coal cloud region. The resulting features are demonstrated to reflect the actual variations in pulverized coal flow. The detection method was evaluated using images from

tuyeres in a blast furnace of SSAB Europe in Raahe, Finland, and the results were found to be generally consistent with research findings and actual operating experience [3,6,7,21,22]. The results provide valuable insights into the relationship between coal combustion status and tuyere conditions, which may be utilized in the future to contribute to the enhanced stability of blast furnace operations.

2. Methodology

The approach developed in the present work is illustrated by the flow chart in Figure 1. First, original images of the tuyere from a CCD camera are preprocessed. Filtering techniques and the Gamma transformation (GT) algorithm are applied to denoise and enhance the tuyere images, respectively. A binary graph of the pulverized coal cloud is then obtained by utilizing the adaptive Otsu thresholding method, which maximally preserves the edge details. The Swin–Unet model is used to segment the pulverized coal cloud, and the obtained regions are processed using the RGB super-pixel weighting method to generate a weighted image of the coal dust cloud. Finally, the combustion state index of the injected coal is quantified based on the results.

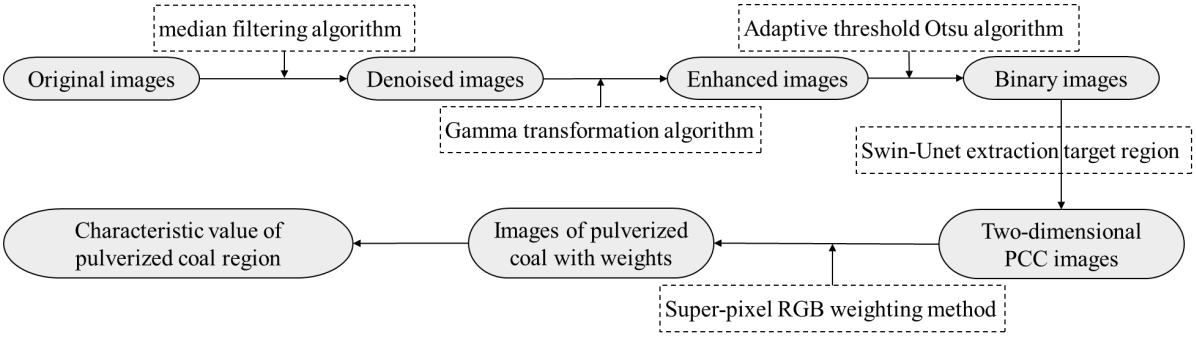


Figure 1. Flowchart of proposed methodology.

The process of extracting tuyere images is depicted schematically in Figure 2. The detection system for an individual tuyere is composed of an image capture unit equipped with a high-resolution CCD camera and a lens-protection device, PC-based image storage, and a processing unit.

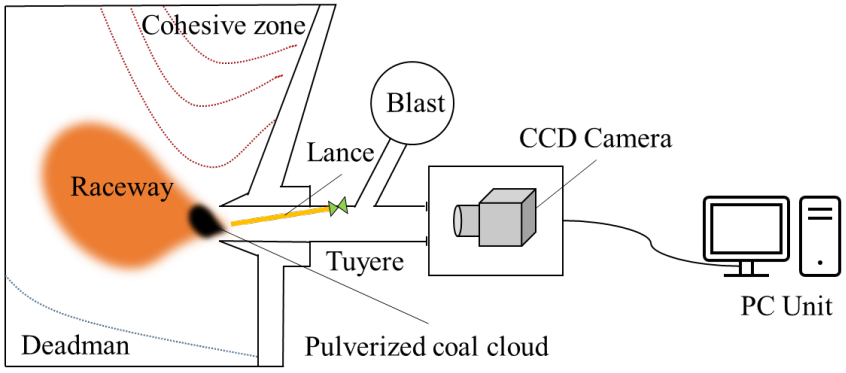


Figure 2. Sketch of the digital imaging system.

Figure 3 shows examples of pictures of the raceway captured by the detection system. The image captured consists of the lance, pulverized coal cloud, raceway, and tuyere wall. Despite the low resolution of the images, it is possible to observe the variations in the shape of the pulverized coal cloud and the changes in tuyere color under different process states. The data used in the present study are form BF1 of SSAB Europe in Raahe, Finland. The main operation parameters of the BF during the test period are reported in Table 1.

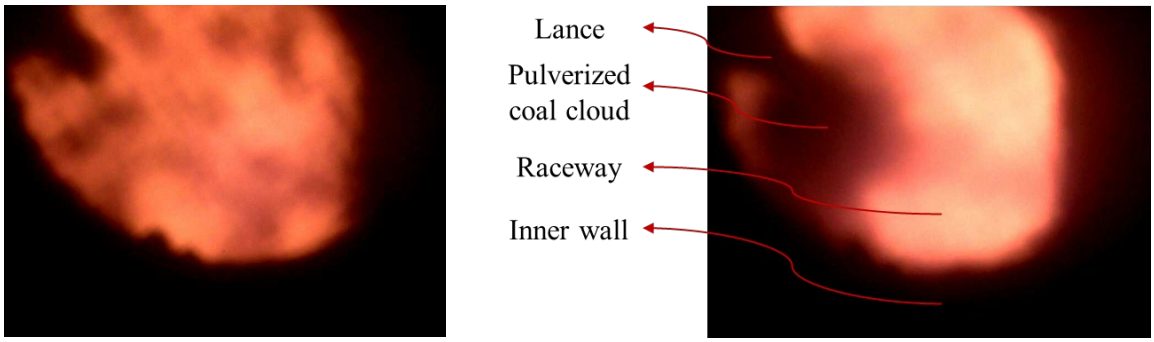


Figure 3. Examples of raceway images. (**a**) No PCI and (**b**) normal PCI operation.

Table 1. Characteristic parameters of the blast furnace studied.

Parameter	Value	Parameter	Value
Working Volume (m^3)	1220	Coke rate (kg/thm)	340
Number of tuyeres	21	PC rate (kg/thm)	140
Blast volume (kNm^3/h)	140	Hot metal production rate (t/d)	3600
Blast temperature (°C)	1100	Hot metal temperature (°C)	1480
Blast oxygen (%)	28	Slag ratio (kg/thm)	200

3. Raceway Image Segmentation and Feature Extraction

3.1. Image Pre-Processing

Tuyere cameras and lenses face a harsh environment characterized by high temperature, intensive radiation in the IR and visible regions, as well as presence of unburned gases and dust during image acquisition and transmission, often leading to degraded image quality and blurriness. The large temperature difference between the lens and the hot blast also leads to a dynamic thermal distortion of the images. To address these challenges, a two-step preprocessing approach was undertaken. Initially, a median filtering algorithm was employed to denoise the images. Median filtering, a non-linear process, replaces each pixel value with the median value of the intensity levels in the neighborhood of that pixel, effectively reducing salt-and-pepper noise while preserving vital image edges. Following the noise reduction, the GT algorithm was applied to further enhance the images. It adjusts the luminance of the images according to [23].

$$S = cr^{\gamma} \quad r \in [0,\ 1] \tag{1}$$

where $r \in [0, 1]$ is the input value of a grayscale image, s is the grayscale output value after GT, c is the grayscale scaling factor and γ is the gamma factor controlling the scaling degree of the whole transformation.

This approach was found to successfully eliminate noise interference in the tuyere image while still preserving important edges, laying a solid foundation for subsequent processing. To achieve a more precise delineation of the pulverized coal cloud region based on the distinctive features of the raceway image, the Otsu algorithm was employed to effectively eliminate the inner wall background and possible coke particles that were seen in the images. Compared to the traditional Otsu algorithm, the adaptive algorithm introduces the concept of local thresholds on the basis of Otsu. By dividing the image into different regions, the algorithm can automatically adjust the threshold according to the local characteristics of the image. This approach allows for the preservation of the edge features of the coal dust cloud while eliminating unnecessary information. By segmenting the image into different regions and applying appropriate thresholds, unnecessary information could be removed while preserving the characteristic edges of the pulverized coal cloud.

Due to the proximity of the RGB values of the pulverized coal cloud to the inner wall where they come into contact, differentiating the boundaries became a challenging task. To address this issue, the edge of the inner wall was determined by utilizing raceway images captured during an all-coke operation, e.g., prior to or after furnace stoppages. This approach was found to feasibly and accurately locate the boundaries of the inner wall; the results of this strategy are illustrated in Figure 4.

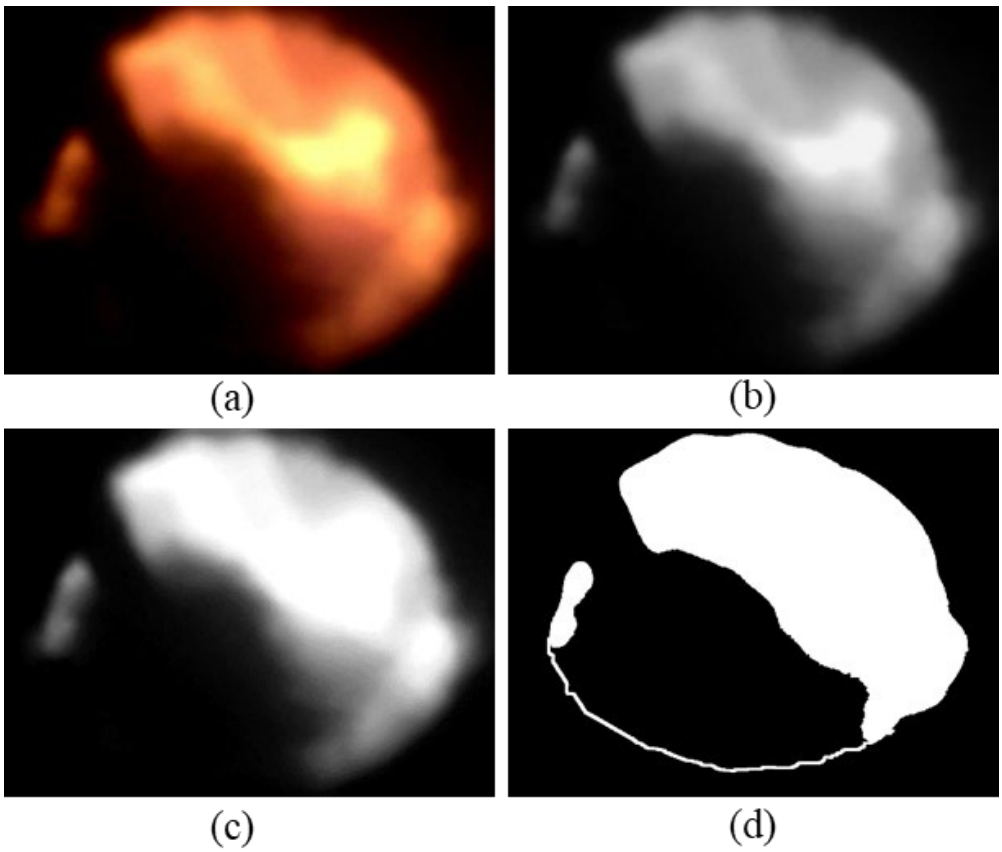


Figure 4. Preprocessing procedures of the raceway image. (**a**) Original image. (**b**) De-noised image. (**c**) Enhanced image. (**d**) Otsu-binarized image.

3.2. Segmentation of the PC Region

After obtaining the position of the pulverized coal cloud, the next step is to extract the coal cloud region. Due to dynamic changes in the position of the lance during the coal injection process, it is not feasible to use a fixed-background plate on the inner wall and lance to determine the shape and position of the pulverized coal cloud. Although CNN-based methods have achieved excellent performance in the field of image segmentation, it is important to note that convolutional neural networks primarily focus on local information. This computational mechanism makes it difficult for them to capture global information and store long-range dependency information. As a result, they may not be fully capable of handling the diverse situations that arise in industrial applications or accurately segmenting pulverized coal clouds in the specific application at hand. Inspired by the self-attention mechanisms introduced in the paper on the Transformer by Vaswani et al. [24], many researchers in the computer vision field have explored the potential of utilizing these mechanisms to capture long-range dependencies in image segmentation tasks and have proposed using self-attention mechanisms to overcome the inherent limitations of CNNs [25,26]. The Vision Transformer (ViT) [27] is based on a complete self-attention transformer architecture and does not rely on CNNs. It divides the image into fixed-size patches and then inputs each patch along with its position information into a linear projection. We apply the transformer-based image segmentation algorithm, Swin–Unet, to

the task of pulverized coal cloud segmentation. By incorporating the Swin Transformer as its core, Swin–Unet harnesses the transformer's self-attention capabilities to effectively understand global contexts and discern detailed features within images. This integration ensures a seamless blend of the Swin Transformer's strength in capturing complex patterns with U-Net's established efficiency in maintaining spatial integrity and precise localization through its symmetric encoder–decoder configuration.

Based on Swin–Unet, the pulverized coal cloud segmentation follows a similar approach to the original U-Net semantic segmentation. Figure 5b shows that Swin–Unet consists of an encoder, a bottleneck, a decoder, and skip connections. The "Patch Merging Block" and "Swin Transformer Block" are two key building blocks in the Swin–Unet. Patch merging is a non-convolutional down-sampling technique, where adjacent patches of size $n \times n$ are grouped and concatenated in the depth dimension. This effectively down-samples the input by a factor of n, transforming the input from a shape of $L \times W \times C$ to $(L/n) \times (W/n) \times (n^2C)$, where L, W, and C refer to the height, width, and channel depth, respectively.

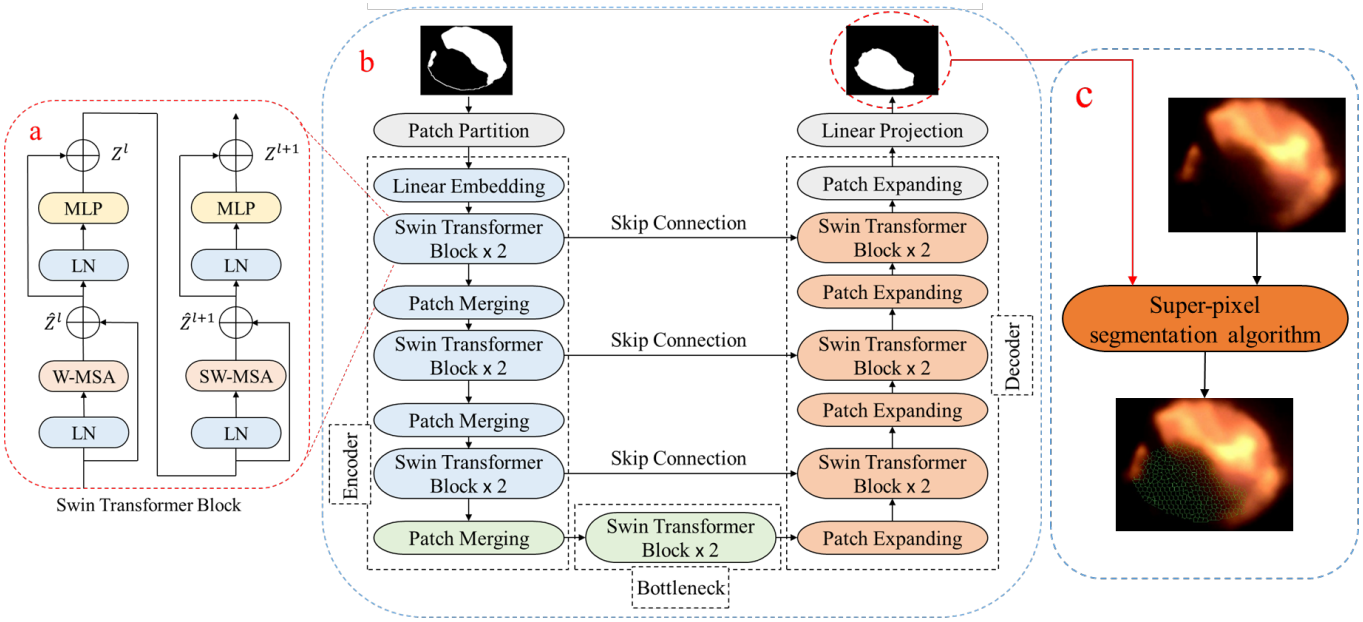


Figure 5. (**a**) Principle of Swin Transformer block. (**b**) Schematic diagram of pulverized coal cloud segmentation by Swi–Unet. (**c**) Schematic of super-pixel extraction.

The Swin Transformer module is based on a shifted window configuration. As shown in Figure 5a, each Swin Transformer block consists of a regular window-based Multi-head Self-Attention (W-MSA) module and a shifted window-based Multi-head Self-Attention (SW-MSA) module, followed by a two-layer MLP with Gaussian Error Linear Units non-linearity. A LayerNorm (LN) layer is applied before each MSA module and MLP, and residual connections are applied after each module. The detailed calculation rules are:

$$\hat{Z}^l = \text{W-MSA}\left(\text{LN}\left(Z^{l-1}\right)\right) + Z^{l-1} \tag{2}$$

$$Z^l = \text{MLP}\left(\text{LN}\left(\hat{Z}^l\right)\right) + \hat{Z}^l \tag{3}$$

$$\hat{Z}^{l+1} = \text{SW-MSA}\left(\text{LN}\left(Z^l\right)\right) + Z^l \tag{4}$$

$$Z^{l+1} = \text{MLP}\left(\text{LN}\left(\hat{Z}^{l+1}\right)\right) + \hat{Z}^{l+1} \tag{5}$$

In the above equations, $\hat{Z}^l$ is the output features of the W-MSA module and SW-MSA module, and Z^l is the output features of the MLP module, where l represents the number of blocks.

The encoder part utilizes the backbone network of the Swin Transformer, which has a four-level hierarchical structure. The minimum structural unit of the Swin Transformer is a 4×4 image patch. After patch segmentation, the input image is reduced to one-quarter of its original size in width and height, and the channel dimension is increased by 16 times. The first layer of the encoder has the same structure as the ViT, using linear embedding connections. It does not change the length and width but doubles the number of channels. In the subsequent three down-sampling layers, the length and width are reduced by half each time, while the channel dimension becomes twice as large. The decoder structure is symmetric to the encoder and uses patch expansion layers for up-sampling. The first three up-sampling layers reshape the low-resolution feature maps into double-resolution feature maps and accordingly reduce the feature dimension to half of the original. To maintain the same size as the input image, the final patch expansion layer performs a four-times up-sampling in length and width without changing the channel dimension. Unlike the Swin Transformer blocks in the encoder, the Swin Transformer blocks in the decoder accept two inputs: the up-sampled features and the skip-connection features. The extracted contextual features are fused with the multi-scale features from the encoder through skip connections to complement the spatial information loss caused by down-sampling.

In summary, the panoramic pulverized coal cloud image is segmented into several non-overlapping image patches, which are then fed into the transformer-based encoder to learn the deep features of the target objects. The decoder and encoder architectures fuse multi-scale feature extraction into the image to complete the segmentation task. The process of extracting the pulverized coal cloud region from a tuyere image is shown in Figure 5b.

3.3. Pulverized Coal Combustion Model

The information obtained about the coal cloud characteristics is only from the two-dimensional area images segmented from the raceway images, where all pixels are extracted with the same weight. However, it is clear that the variation in the number of pixels or the change in the projected area does not necessarily reflect the variation in the amount of pulverized coal injected. From the original images, it was observed that the density of the coal cloud increases as its central region is approached, while the opposite holds true for the edges of the cloud. Based on the variations in RGB values at each pixel position, we therefore propose a super-pixel RGB weighting method. This approach utilizes the varied colors within the pulverized coal plume by applying weights to each pixel within the region. This proved to yield a more accurate representation of the pulverized coal plume.

Firstly, the coal cloud region was segmented using the SLIC super-pixel segmentation algorithm. Next, the RGB values were converted to grayscale, and the grayscale value of each super-pixel was calculated by:

$$H = 0.299R + 0.587G + 0.114B \tag{6}$$

which involves the cluster center grayscale value and the average grayscale value within the super-pixel. The weight of each super-pixel was next determined by:

$$H_{\text{slic}} = \alpha H_{\text{center}} + (1 - \alpha) H_{\text{aver}} \tag{7}$$

$$F(H) = 1 - (H_{\text{slic}} - H_{\text{min}}) / (H_{\text{max}} - H_{\text{slic}}) \tag{8}$$

where H is the gray value of the pixel, H_{slic} represents the theoretical grayscale value of a super-pixel, H_{center} the grey value of cluster center in the super-pixel, and H_{aver} the average grey value in the super-pixel, while H_{max} and H_{min} are the maximum and minimum grey

value, respectively, in the areas of the pulverized coal plume. In this work, $\alpha = 0.6$ was used in the filter.

Finally, the number of pixels was multiplied by the weight of each super-pixel region to yield a variable, M, that was taken to represent the characteristic value of pulverized coal. This variable was found to reflect the change in the pulverized coal clouds in the images. A schematic of the super-pixel extraction is provided in Figure 5c.

3.4. Implementation and Training Details of Model

The Swin–Unet was implemented with Python 3.8 in the Pytorch framework and a NVIDIA GTX-3080Ti GPU was used for training. The experimental dataset consisted of 8000 raceway images, of which 80% were randomly selected for the training set, while the remaining ones were used as the test set. The pulverized coal region in the images was manually detected and labeled as the ground truth, and this acted as the target area for the Swin–Unet algorithm; other areas were considered as the background. All pixel values in the ground truths were thus binary labeled, indicating that a pixel either belongs (1) or does not belong (0) to the pulverized coal cloud. The network utilized binary cross entropy as the loss function and employed the Adam optimization algorithm with a learning rate of 0.001. The model achieved convergence after approximately 130 epochs, which took about 5 h of training time.

4. Results and Discussions

4.1. Evaluation of the Segmentation of Coal Region Analysis

Figure 6a shows examples of images of three different tuyeres and an image of one of the tuyeres (#10) at another moment in time. It can be seen that the positions of the lances are different and also that the position of the tuyere camera lens may vary with time. Binary images obtained after preprocessing are shown in Figure 6b. The Swin–Unet extraction model (Figure 6c,d) successfully captures the region of the pulverized coal cloud with accurate segmentation, satisfying the requirements for further analysis and computation.

To evaluate the accuracy of the proposed model, Mean Intersection over Union (MIoU) and pixel accuracy (PA) were used as metrics. The former is defined as:

$$\mathrm{MIoU} = \frac{1}{k+1}\sum_{i=0}^{k}\frac{p_{ii}}{\sum_{j=0}^{k} p_{ij} + \sum_{j=0}^{k} p_{ji} - p_{ii}} \tag{9}$$

PA is a simple indicator expressing the ratio between the number of pixels correctly classified and the total number of pixels.

$$\mathrm{PA} = \frac{\sum_{i=0}^{k} p_{ii}}{\sum_{i=0}^{k}\sum_{j=0}^{k} p_{ij}} \tag{10}$$

where $k+1$ represents the number of categories of contours, including k target classes and one background class, p_{ij} represents the total number of pixels that belong to class i but are predicted as class j. Specifically, p_{ii} represents true positives, while p_{ij} and p_{ji} are usually labeled as false positives and false negatives, respectively.

An evaluation of the results of using the Swin–Unet semantic segmentation model on the pulverized coal cloud dataset are presented in Table 2, which compares it with the performance of some classical CNN-based networks, such as U-Net and DeeplabV3+. The Swin–Unet method is seen to outperform the CNN-based methods in each evaluation metric. Swin–Unet achieved accuracy rates of 97.3% and 98.7% in terms of MIoU and PA, respectively. It was observed that the segmented pulverized coal cloud area was almost identical to the target area, meeting the requirements for a successful application of the method in the blast furnace process.

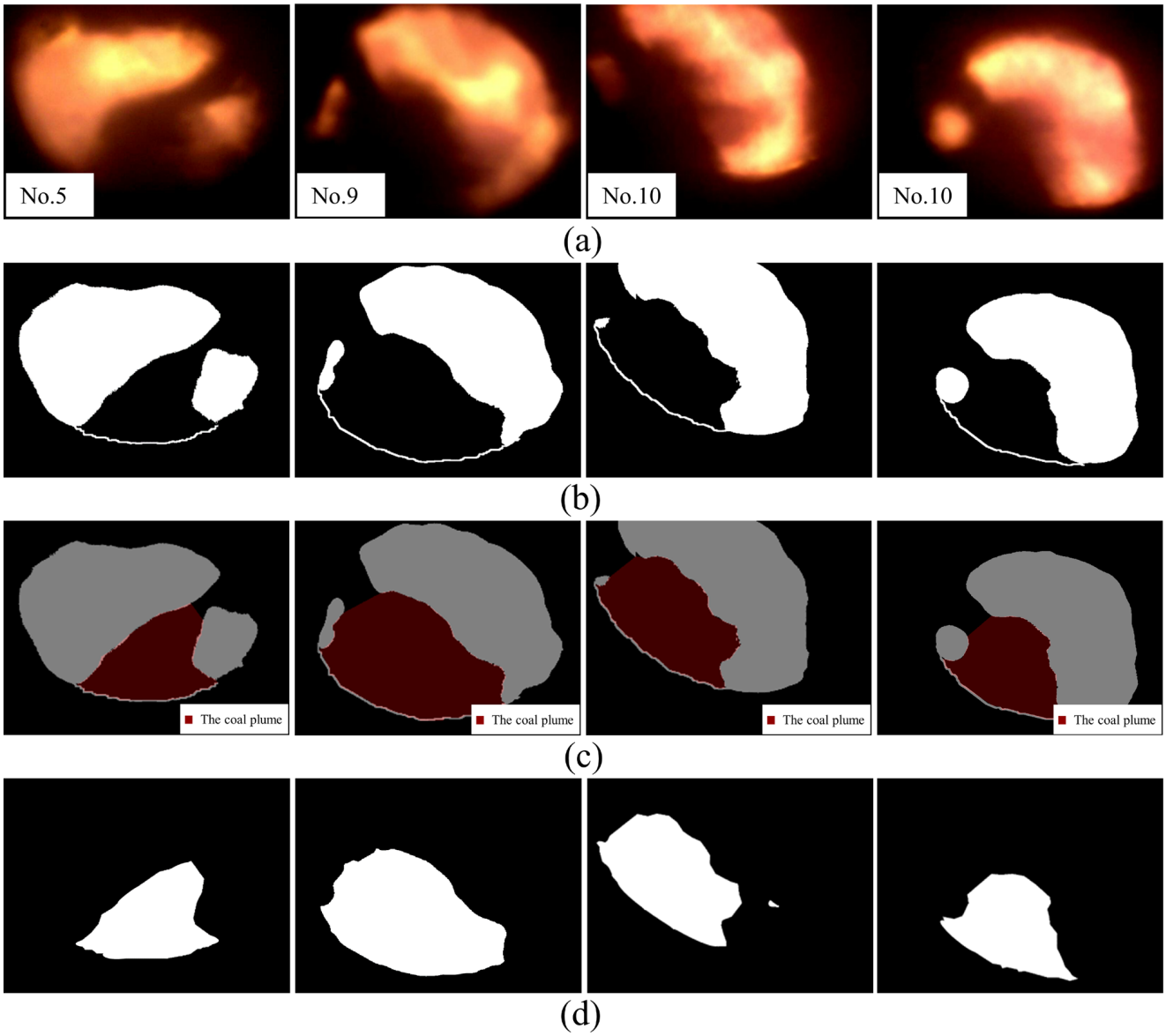


Figure 6. (**a**) Original image from some tuyeres; (**b**) binary images; (**c**) cloud region detection; (**d**) extraction of pulverized coal cloud.

Table 2. Performance comparison of different methods for cloud segmentation.

Item	MIoU (%)	PA (%)
Unet	95.6	96.0
DeeplabV3+	93.9	94.8
Swin–Unet	97.3	98.7

Figure 7 shows examples of the super-pixel effect diagram created by the method, where the green grid regions in the images represent the calculation areas for the weight of the pulverized coal cloud. The weight setting area basically covers the pulverized coal cloud region, which aligns with the expected model outcome.

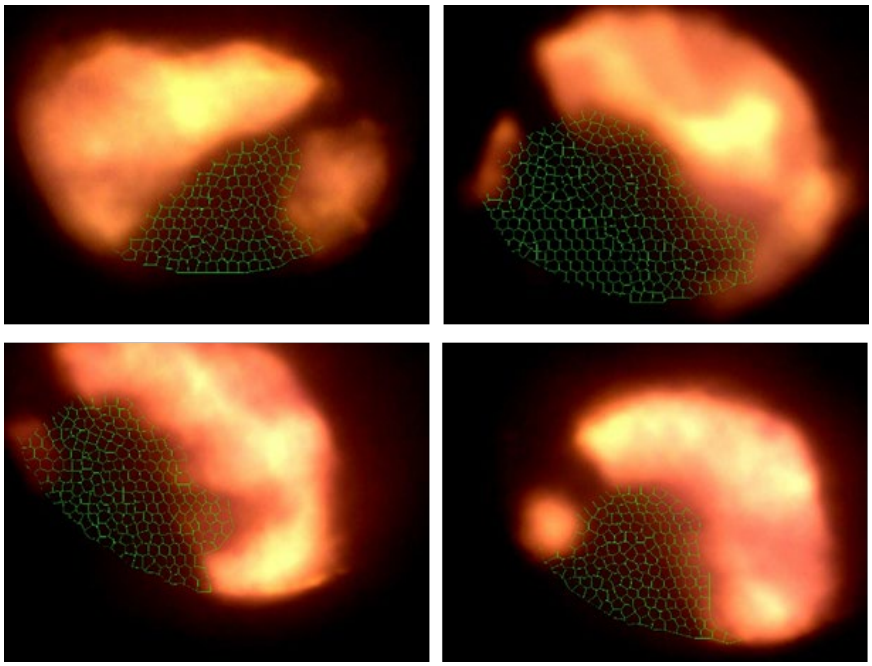


Figure 7. Super-pixel segmentation result image.

4.2. Impact of Injection Rate on Coal Cloud Characteristics

The efficacy of the proposed method is next illustrated by applying it to data from a period of the BF1 of SAAB Europe with a 10 h stoppage, as seen in Figure 8 which depicts the blast volume. Specific attention will be focused on the period after the stoppage, when the target values of the blast volume and pulverized coal rate are gradually recovered, dividing the subperiod into different stages. From each stage, four tuyere images were randomly selected, illustrating, in Figure 9, the impact of the different conditions on the size and morphology of the pulverized coal cloud in the tuyere area. These images capture the dynamic characteristics of the combustion process and highlight the complex interactions between blast volume, PC injection rate, and the dispersion of coal particles. Even though a manual inspection of the images can reveal certain features it is difficult for humans to accurately determine the quality of the plume. Furthermore, the task of simultaneously observing and interpreting images from tens of tuyeres is clearly not feasible for the BF operators.

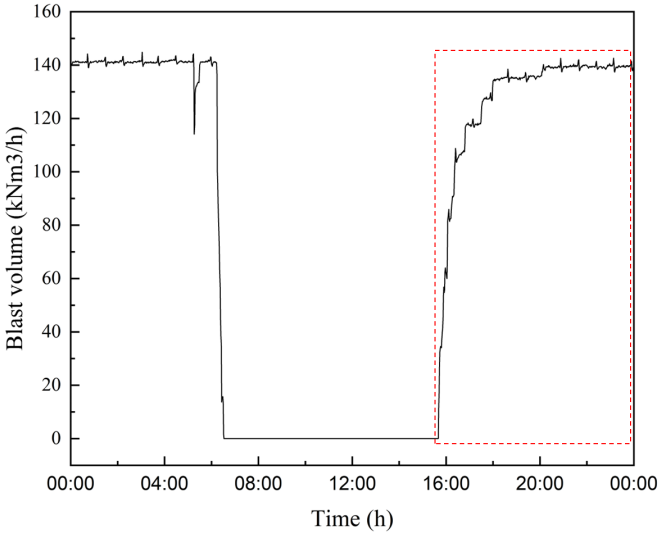


Figure 8. Blast volume in BF1. The period bounded by the dashed region is studied in more detail.

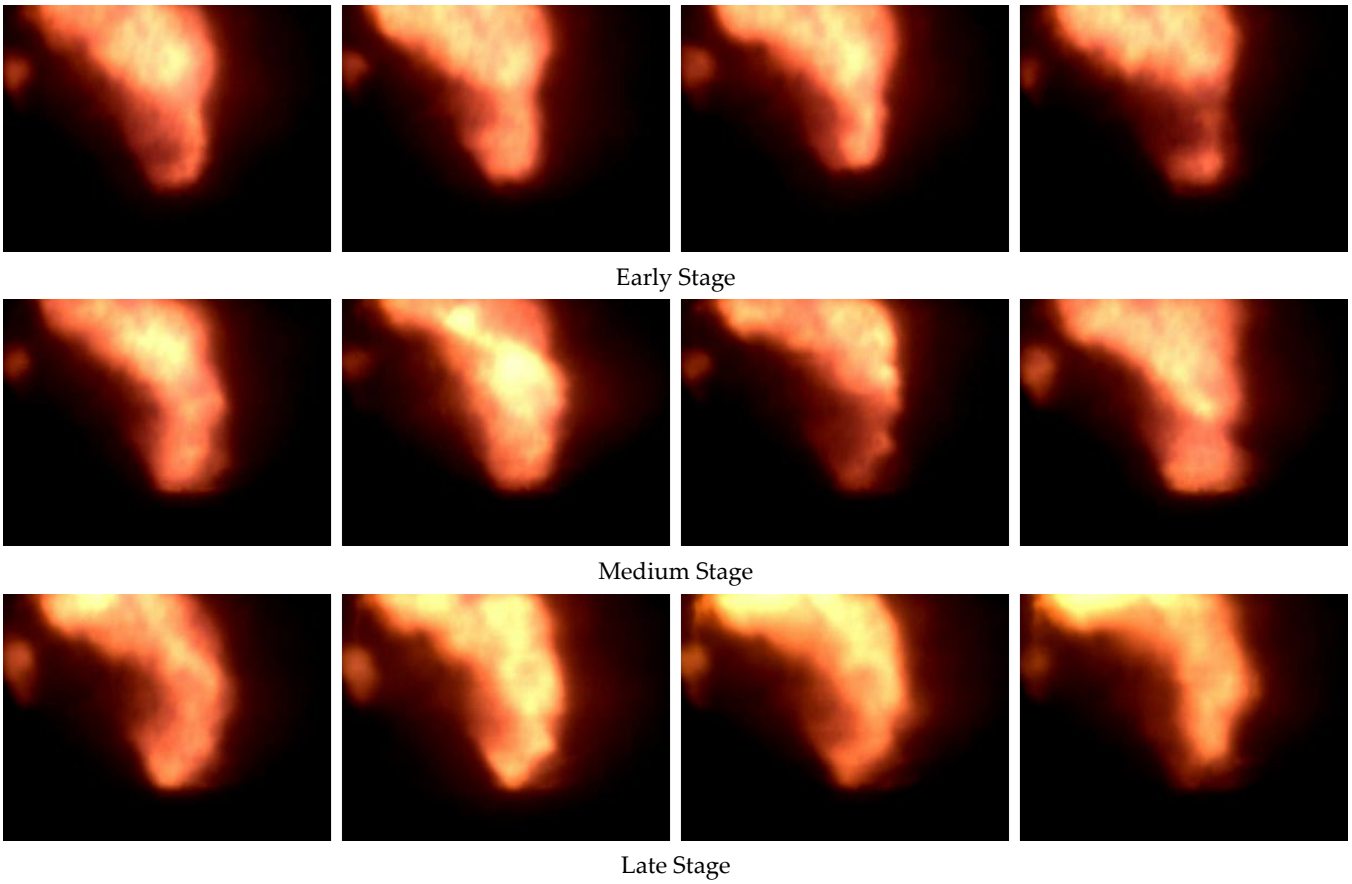


Figure 9. Images of tuyere #10 in BF1 during the recovery period (depicted by the red dashed box in Figure 8).

To demonstrate the performance of the method in assessing the pulverized coal cloud state, it was applied on images from tuyere #10 during the period of "recovery" (dashed box in Figure 8) of the normal operation state after the stoppage. Estimates of the individual flow rates of the blast and PC to the tuyeres were provided by SSAB based on indirect measurements. As seen in Figure 10, during this time, the blast volume (bottom panel) increased from 0 Nm^3/h to 6000 Nm^3/h, and the PCI rate (middle panel) rose from 0 kg/h to 2000 kg/h. Before the coal injection was resumed, the characteristic value M remained consistently near 0. With the increase in PCI, M also surged, fluctuating within a defined range. Utilizing Pearson's correlation coefficient formula, the correlation coefficient between the pulverized coal injection rate and M for the tuyere in question was 0.83 during the period, demonstrating the interdependence between the two variables. It should be noted that the combustion process is complex and depends on both the fuel (coal) and oxidizer (blast), and the mixing of them.

Overall, the results align with our practical observations, highlighting the impact of blast and tuyere injection rates on the coal plume as captured by tuyere camera images. The ability to convert an image into a quantifiable measure that can be easily monitored over time and correlated with other process variables stands out as a significant advantage. However, while the model shows a robust performance in segmenting the coal cloud area, its ability to generalize across the varied production environments of different blast furnaces or under diverse operating conditions requires further validation. Future efforts will be directed towards testing and refining the model in a wider array of conditions to bolster its robustness and applicability.

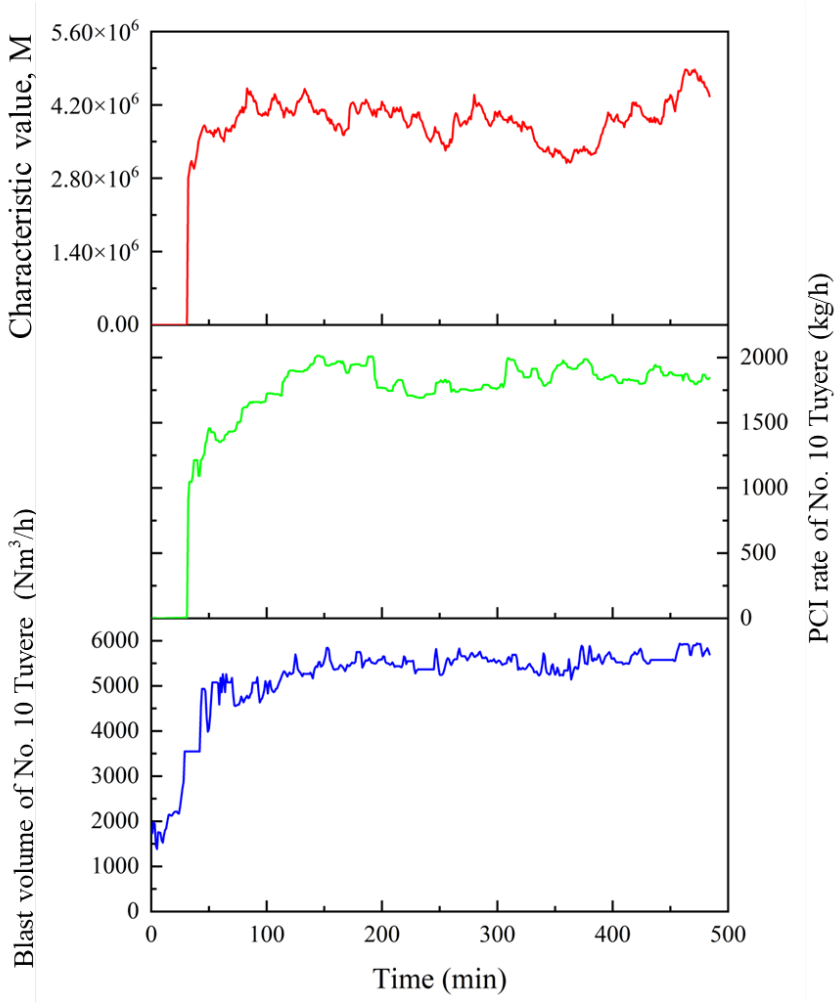


Figure 10. Individual blast volume (bottom panel) and PCI rate (middle panel) to tuyere #10, as well as characteristic value *M* during the period after the stoppage (cf. Figure 8).

5. Conclusions

This study has proposed an image processing and segmentation method to assess the state of the pulverized coal cloud in the tuyere region of the ironmaking blast furnace based on images taken by tuyeres cameras. First, a filtering algorithm was used followed by the application of the Gamma transformation algorithm to denoise and enhance the tuyere images, utilizing the adaptive Otsu thresholding method to delineate the edges of the pulverized coal cloud. The resulting binary images act as the starting point for the subsequent processing. The Swin–Unet model was trained on a sufficient number of such binary images to detect the pulverized coal cloud region. Finally, a characteristic value, *M*, reflecting the coal cloud state was calculated using RGB super-pixel weighting. The model was applied to tuyere images from blast furnace 1 of SSAB Europe in Raahe, Finland, and it was found to provide accurate segment detection and a quantification of the cloud which correlated with the injection conditions in the tuyeres for a period where the blast and coal injection were gradually increased after a stoppage of the furnace. The results of the study hold promise for a future application of the technique for automatic and continuous assessments of the pulverized coal injection state at the tuyeres, facilitating an on-line monitoring of the tuyere/raceway region. Since the setup of tuyere cameras is similar in most steelworks, the method developed is expected to be readily applicable to other blast furnaces with pulverized coal injection.

It should be emphasized that the current research represents initial efforts to apply deep learning techniques to extract information about the state of the combustion zones in

the blast furnace, so further developments are required to ensure the generic applicability of the technique and to explore how to extract additional information from the images, e.g., focusing on the regions representing the raceway after masking out the coal plume and tuyere walls. After detecting the cloud, the raceway region can be better analyzed, which is useful for estimating, e.g., the raceway temperature. Initial trials (not reported in the paper) have already demonstrated that such step-wise processing is promising. Furthermore, a deeper analysis of simultaneous images from multiple tuyeres of the same furnace will be studied for a much longer time period to cover different furnace states. This will also give information about possible imbalance in the supply of coal and blast and provide a more general view of the thermal state of the furnace.

Author Contributions: Conceptualization, G.Z. and H.S.; methodology, G.Z.; software, G.Z.; validation, G.Z.; formal analysis, G.Z. and H.S.; investigation, G.Z. and O.M.; resources, H.S. and O.M.; writing—original draft preparation, G.Z.; writing—review and editing, H.S., Y.Y., O.M. and G.Z.; visualization, G.Z.; supervision, H.S.; project administration, H.S.; funding acquisition, H.S. and Y.Y. All authors have read and agreed to the published version of the manuscript.

Funding: This research was funded by China Scholarship Council, grant number 202106890010.

Data Availability Statement: The raw/processed data required to reproduce these findings cannot be shared at this time as the data also forms part of an ongoing study.

Conflicts of Interest: Author Olli Mattila was employed by the company SSAB Europe Oy. The remaining authors declare that the research was conducted in the absence of any commercial or financial relationships that could be construed as a potential conflict of interest.

Abbreviations

BF	Blast furnace
PC	Pulverized coal
PCI	Pulverized coal injection
CNN	Convolutional neural network
GT	Gamma transformation
ViT	Vision Transformer
W-MSA	Window-based Multi-head Self-Attention
SW-MSA	Shifted Window-based Multi-head Self-Attention
LN	Layer Normalization
MLP	Multi-Layer Perceptron

References

1. Agrawal, A.; Tiwari, R.K.; Kumar, S.; Chatterjee, R.; Singh, B.K.; Singh, R.S.; Tripathi, V.R.; Kundu, S.; Padmapal; Ramna, R.V.; et al. Technological Advancements in Evaluating the Performance of the Pulverized Coal Injection through Tuyeres in Blast Furnace. *Metall. Res. Technol.* **2020**, *117*, 611–633. [CrossRef]
2. Shen, Y.S.; Yu, A.B.; Austin, P.R.; Zulli, P. CFD Study of In-Furnace Phenomena of Pulverised Coal Injection in Blast Furnace: Effects of Operating Conditions. *Powder Technol.* **2012**, *223*, 27–38. [CrossRef]
3. Zhuo, Y.; Shen, Y. Transient 3D CFD Study of Pulverised Coal Combustion and Coke Combustion in a Blast Furnace: Effect of Blast Conditions. *Fuel* **2023**, *340*, 127468. [CrossRef]
4. Liu, L.; Kuang, S.; Jiao, L.; Guo, B.; Yu, A. Optimization of Pulverized Coal Injection (PCI) Rate in an Ironmaking Blast Furnace by an Integrated Process Model. *Fuel* **2022**, *315*, 122832. [CrossRef]
5. Dianyu, E.; Zhou, P.; Guo, S.; Zeng, J.; Xu, Q.; Guo, L.; Hou, Q.; Yu, A. Particle-Scale Study of Coke Combustion in the Raceway of an Ironmaking Blast Furnace. *Fuel* **2022**, *311*, 122490. [CrossRef]
6. Straka, R.; Bernasowski, M.; Klimczyk, A.; Stachura, R.; Svyetlichnyy, D. Prediction of Raceway Shape in Zinc Blast Furnace under the Different Blast Parameters. *Energy* **2020**, *207*, 118153. [CrossRef]
7. Du, S.W.; Chen, W.H.; Lucas, J.A. Pulverized Coal Burnout in Blast Furnace Simulated by a Drop Tube Furnace. *Energy* **2010**, *35*, 576–581. [CrossRef]
8. Zhou, D.; Xu, K.; Bai, J.; He, D. On-Line Detecting the Tuyere Coke Size and Temperature Distribution of Raceway Zone in a Working Blast Furnace. *Fuel* **2022**, *316*, 123349. [CrossRef]
9. Zhou, D.; Cheng, S. Measurement Study of the PCI Process on the Temperature Distribution in Raceway Zone of Blast Furnace by Using Digital Imaging Techniques. *Energy* **2019**, *174*, 814–822. [CrossRef]

10. Cheng, X.; Cheng, S.; Liu, K.; Zhou, D. Measurement Study of Preheated Pulverized Coal Injection on Combustion in a Blast Furnace Raceway by Visual Detection. *Fuel* **2020**, *271*, 117626. [CrossRef]
11. Li, Y.; Cheng, S.; Zhang, R.; Zhou, D.; Chen, T. Reconstruction of Three-Dimensional Temperature Distribution with Radiative Image by Monte Carlo Method in Blast Furnace Raceway. *ISIJ Int.* **2017**, *57*, 2141–2147. [CrossRef]
12. Zhang, R.; Cheng, S.; Guo, C. Detection Method for Pulverized Coal Injection and Particles in the Tuyere Raceway Using Image Processing. *ISIJ Int.* **2018**, *58*, 244–252. [CrossRef]
13. Huang, P.; Zhao, J.; Wang, Y. A Visual Detection Method for PCI Blockage and Coke Size Distribution in Tuyere Raceway. *Ironmak. Steelmak.* **2021**, *48*, 919–926. [CrossRef]
14. Wang, Y.; Huang, P.; Yang, G. A Visual PCI Blockage Detection in Blast Furnace Raceway. *ISIJ Int.* **2020**, *60*, 519–527. [CrossRef]
15. Olaf, R.; Philipp, F.; Thomas, B. U-Net: Convolutional Networks for Biomedical Image Segmentation. In Proceedings of the Medical Image Computing and Computer-Assisted Intervention, Munich, Germany, 5–9 October 2015.
16. Simonyan, K.; Zisserman, A. Very Deep Convolutional Networks for Large-Scale Image Recognition. *arXiv* **2014**, arXiv:1409.1556. [CrossRef]
17. Krizhevsky, A.; Sutskever, I.; Hinton, G.E. ImageNet Classification with Deep Convolutional Neural Networks. *Commun. ACM* **2017**, *60*, 84–90. [CrossRef]
18. Zheng, S.; Lu, J.; Zhao, H.; Zhu, X.; Luo, Z.; Wang, Y.; Fu, Y.; Feng, J.; Xiang, T.; Torr, P.H.S.; et al. Rethinking Semantic Segmentation from a Sequence-to-Sequence Perspective with Transformers. In Proceedings of the CVF Conference on Computer Vision and Pattern Recognition, Nashville, TN, USA, 19–25 July 2020.
19. Xiao, H.; Li, L.; Liu, Q.; Zhu, X.; Zhang, Q. Transformers in Medical Image Segmentation: A Review. *Biomed. Signal Process. Control* **2023**, *84*, 104791. [CrossRef]
20. Cao, H.; Wang, Y.; Chen, J.; Jiang, D.; Zhang, X.; Tian, Q.; Wang, M. Swin-Unet: Unet-like Pure Transformer for Medical Image Segmentation. In Proceedings of the European Conference on Computer Vision, Tel Aviv, Israel, 23–27 October 2021.
21. Li, W.; Zhuo, Y.; Bao, J.; Shen, Y. A Data-Based Soft-Sensor Approach to Estimating Raceway Depth in Ironmaking Blast Furnaces. *Powder Technol.* **2021**, *390*, 529–538. [CrossRef]
22. Wu, D.; Zhou, P.; Zhou, C.Q. Evaluation of Pulverized Coal Utilization in a Blast Furnace by Numerical Simulation and Grey Relational Analysis. *Appl. Energy* **2019**, *250*, 1686–1695. [CrossRef]
23. Chourasiya, A.; Khare, N. A Comprehensive Review Of Image Enhancement Techniques. *Int. J. Innov. Res. Growth* **2019**, *8*, 60–71. [CrossRef]
24. Vaswani, A.; Brain, G.; Shazeer, N.; Parmar, N.; Uszkoreit, J.; Jones, L.; Gomez, A.N.; Kaiser, Ł.; Polosukhin, I. Attention Is All You Need. In Proceedings of the Neural Information Processing Systems, Long Beach, CA, USA, 4–9 December 2017.
25. Wang, X.; Girshick, R.; Gupta, A.; He, K. Non-Local Neural Networks. In Proceedings of the IEEE/CVF Conference on Computer Vision and Pattern Recognition, Salt Lake City, UT, USA, 18–23 June 2018.
26. Chen, J.; Lu, Y.; Yu, Q.; Luo, X.; Adeli, E.; Wang, Y.; Lu, L.; Yuille, A.L.; Zhou, Y. TransUNet: Transformers Make Strong Encoders for Medical Image Segmentation. *arXiv* **2018**, arXiv:2102.04306.
27. Dosovitskiy, A.; Beyer, L.; Kolesnikov, A.; Weissenborn, D.; Zhai, X.; Unterthiner, T.; Dehghani, M.; Minderer, M.; Heigold, G.; Gelly, S.; et al. An Image Is Worth 16 × 16 Words: Transformers for Image Recognition at Scale. *arXiv* **2021**, arXiv:2010.11929.

Disclaimer/Publisher's Note: The statements, opinions and data contained in all publications are solely those of the individual author(s) and contributor(s) and not of MDPI and/or the editor(s). MDPI and/or the editor(s) disclaim responsibility for any injury to people or property resulting from any ideas, methods, instructions or products referred to in the content.